JOURNAL OF MATERIALS SCIENCE 27 (1992) 2743–2748

X-ray diffraction study of small laser-treated spots on WC–Co hardmetal

M. ERMRICH*, D. STEPHAN, B. SCHULTRICH
Institute of Structure Research and Solid State Physics, Helmholtzstrasse 20, 0-8027 Dresden, Germany

The influence of laser treatment on phase transformation and stability of WC–6%Co hardmetal was investigated by X-ray diffraction. The sample was irradiated by a neodymium–glass laser ($\lambda = 1.06\ \mu m$) with different energy densities. The high-temperature β-WC_z phase (stable above 2500 °C) was frozen without any decay in α-WC and W_2C. The strict stoichiometry of α-WC up to high temperatures is shown, because the observed changes in lattice parameters could be attributed to different residual stress states. Therefore, the nondilated direction method was used. The degree of decarburization in the laser spot has been estimated. To obtain material information about regions of 3 mm^2 down to 0.04 mm^2, the advantages of both a position-sensitive detector and a microdiffractometer connected to an annular proportional counter, were used.

1. Introduction

Laser treatment of materials is a well-established method for improving wear resistance and hardness of localized surface regions. These effects are based on nonequilibrium states frozen by self-quenching. Of special interest for material science are composite materials of the hardmetal type which take an intermediate position between metals and ceramics. With special laser irradiation conditions, a further increase of hardness of these already hard materials could be achieved [1]. The essential role of the binder phase in these processes was proved in a WC hardmetal using direct irradiation inside a scanning electron microscope. Schultrich and co-workers [2–4] have shown that the formation of the "molten layer" on the surface at intense irradiation results from stimulated dissolution in the lower melting binder. The rise in hardness was at least partially caused by solid solution and precipitation hardening of the binder phase, oversaturated with, for example, tungsten and carbon. But in comparison to this, the laser-induced processes of the carbide phases have been little investigated.

WC (apart from its practical importance in tool materials) is especially suited for such investigations: the standard phase, hexagonal α-WC, is strictly stoichiometric (at least at not too high temperatures), hence carbon deficiences can be clearly detected. Furthermore, there exist two additional phases with a broader stoichiometric region, the hexagonal W_2C and the cubic high-temperature phase, β-WC_z, stable only above 2500 °C, thus setting a clear temperature mark (see Fig. 1).

The problems arising in the detailed investigations of these phases follow from the small dimensions of the irradiated areas and required advanced X-ray methods. Therefore it was the aim of this work to use the advantages of a position-sensitive detector (PSD) and a microdiffractometer connected to an annular proportional counter (APC), to answer the following questions.

1. Does a correlation exist between the appearance of new phases and topological changes of the surface?
2. Is the cubic β-WC_z stable down to room temperature or does it partially decay into α-WC and W_2C?
3. Is the strict stoichiometry of the α-WC phase valid up to high temperatures?
4. What is the degree of decarburization?

2. Experimental procedure

The investigated WC–6%Co hardmetal was produced by the usual powder metallurgy. The carbide grain sizes were about 1 μm. The surface region was intensively plastified by grinding which leads to compressive stresses of the order of 1 GPa [5]. The sample was irradiated with a neodymium–glass laser ($\lambda = 1.06\ \mu m$, pulse energy ~ 5 J, pulse length ~ 5 ms). For spots of some millimetres in size the energy density is of the order 100 $J\,cm^{-2}$. Different laser irradiation intensities were achieved by varying the distance from the focal plane. In this way laser spots (I, II, III, see Fig. 2) with diameters of about 2.8, 3.5 and 4 mm, were produced corresponding to relations of energy density of 2:1.3:1, respectively. A more detailed investigation [1] should take into consideration the inhomogeneous energy distribution in the laser beam. The energy profile was nearly gaussian-shaped with some irregularities in the spot centre.

* *Present address*: STOE and CIE GmbH, Hilpertstrasse 10, D-6100 Darmstadt, Germany.

0022–2461

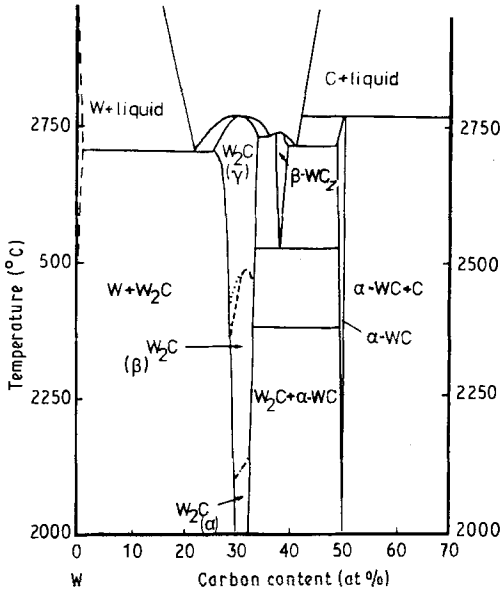

Figure 1 Phase diagram after Rudy and Hoffmann [10]. According to the results of the present work, no finite region of stoichiometry was detectable for α-WC up to the melting point, so the region shown should be replaced by a line.

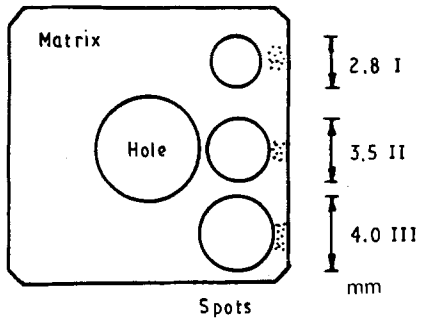

Figure 2 Drawing of the hardmetal showing laser spots I, II, III.

The mechanical and electrical parameters of our PSD and its application to comprehensive investigations in X-ray diffractometry have been described previously [6, 7]. The simultaneously detected Bragg-angle region is about $\Delta 2\theta = 9.2°$ for a given sample-to-detector distance of 250 mm. The measurements were carried out using CoK_α radiation. The observed area of the sample was about 3 mm^2. Smaller areas of 0.5–0.04 mm^2 were observed at the microdiffractometer with APC and a special optical alignment. For the diagram registration, the sample is moved to the detector, so thus the detector observed the different Debye–Scherrer cones versus the distance APC–sample, s, see Fig. 3. The cross-section of the primary beam is formed by an X-ray tube with a normal point focus and a pin-hole of about 0.15 mm diameter. Stephan and Richter [8] described both parameters and an application of the APC-diffractometer. The backscattering arrangement ($\Delta\theta = 65°$–$85°$) is favourable for stress measurements and precision determination of lattice parameters. The measurements were carried out using FeK_α and CoK_α radiation.

3. Results and discussion

The starting WC–Co hardmetal (matrix M) after sintering and grinding, consists of hexagonal α-WC and cubic Co. The sample shows the usual appearance of a roughly ground surface where the structure of the material is overlaid by deformed cobalt binder smeared over the surface and the engraved traces of grinding (Fig. 4).

After treatment, the laser-irradiated regions are clearly visible as bright circles. For Spot I with the most concentrated laser irradiation inside the spot, an irregular dark region appears (see Fig. 5a). These two regions are the low-temperature area (LTA) and the high temperature area (HTA). The microscopic investigations of the LTA show that the covering of cobalt film has disappeared here, thus disclosing the carbide grains (see Fig. 5b). In the HTA, a connected layer of molten material was formed with pores from the intense evaporation processes (see Fig. 5c).

The results of the qualitative phase analysis by PSD of the three laser spots are shown in Fig. 6. The simultaneously detected reflections of the α-WC (1 0 0), the cubic β-WC_z (1 1 1) and the hexagonal W_2C (0 0 2) are plotted. Only in the laser Spot I was a phase transition into W_2C and the high-temperature phase β-WC_z, observed. This means that a temperature of at least 2500 °C was attained during laser treatment (Fig. 1).

These results were confirmed by the APC measurements. In Fig. 7a the diagrams from the matrix, M, and the regions LTA and HTA of Spot I are plotted

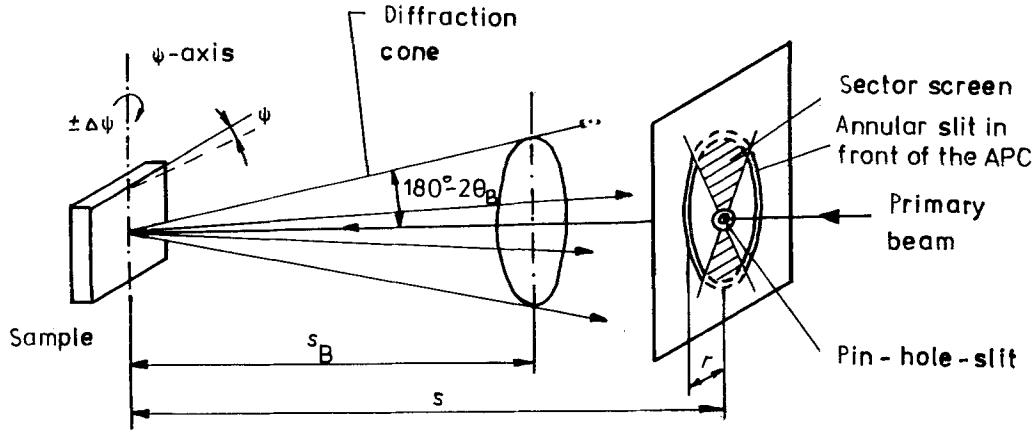

Figure 3 The schematic arrangement of the micro diffractometer with the annular proportional counter (APC), in the case of local phase analysis after Stephan and Richter [8].

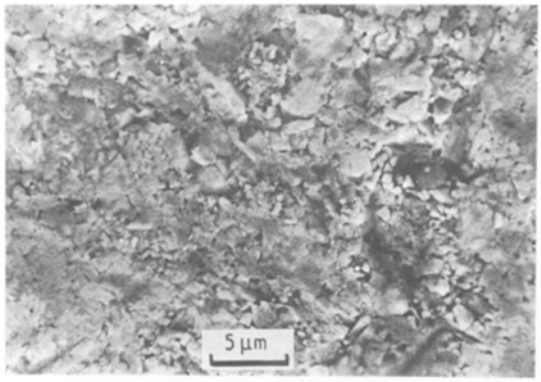

Figure 4 Scanning electron micrograph of the ground surface (matrix) before laser irradiation. WC grains are partially cracked and covered with a thin cobalt film.

versus the distance, s, between the sample and the annular slit plane of the APC. The observed sample region was only 0.2 mm diameter.

To obtain more detailed information concerning the phase distribution of these two new phases in Spot I, the sample was moved in steps of $\Delta y = 0.1$ mm for a fixed s for each phase (see Fig. 7b). From these local measurements it follows that in the (dark) molten HTA region the original α-WC has been replaced completely by the high-temperature phases W_2C and β-WC_z. Note that no decay of β-WC_z into α-WC and W_2C was found. This show that (i) the high-temperature two-phase state was frozen and (ii) a decarburization of the carbide phases has occurred.

The fluctuation of the maximum of the β-WC_z (4 0 0) reflection indicates the coarse-grained state of this phase. The full width at the half maximum (FWHM) of the α-WC (1 1 2) reflection in the LTA of the spots is generally smaller than in the matrix due to a tempering effect in this region.

To investigate the stoichiometry of the α-WC, the lattice parameters were determined at first with the Bragg–Brentano geometry and the PSD using the (1 1 2) and (2 0 1) reflections. The parameters a and c for the matrix and the LTA zones of the spots are given in Table I ($\Delta a = \Delta c \pm 0.0001$ nm). The values of α-WC powder are also shown, determined with the reflections (0 3 1), (1 1 3) and (1 2 2). To test the strong stoichiometry of the tempered hexagonal α-WC, different amounts of carbon and W_2C were mixed in. However, only more or less W_2C or carbon was observed as additional phases and no changes of the lattice parameters of α-WC were seen. Nevertheless, the different values of these lattice parameters of α-WC for the matrix and the spots shown in Table I seems to be caused by the effects of stoichiometry. The more precise values of the lattice spacing d(1 1 2) measured by APC with a symmetrical sample arrangement at $\psi = 0°$ also do not agree with the powder values.

However, the apparent lattice parameters must be corrected for residual stress. Then we can investigate the influence of chemical effects on the exact stoichiometry in the LTA region. On the one hand there exist grinding stresses in the matrix, but on the other hand, the cracks of Spot I (see Fig. 5a) show the existence of originally tensile stress in this region.

Therefore, at first, local stress measurements following the $\sin^2\psi$ method were carried out (reflection α-WC (1 1 2)); an overview was possible by PSD investigations, with more detailed information obtained by the APC equipment. The angle ψ is defined usually as the angle between the surface of the sample and the diffracting lattice plane. After a linear regression of the measured points $s(\psi)$ the slope b_1 of this line $s = b_0 + b_1 \sin^2\psi$ gives the value of the residual stress (see Fig. 8a). The strong compressive stress (about 2 MPa) of the matrix proceeds to tensile stress (0.8 MPa) in Spot III and small compressive stress in Spot II and the LTA region of Spot I. The point of intersection, $b_0 = s(0)$, finally corresponds to the observed parameters in Table I.

The elimination of the influence of stress is possible by the method of the nondilated direction described

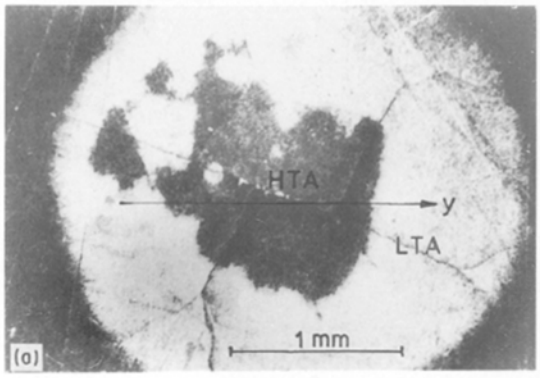

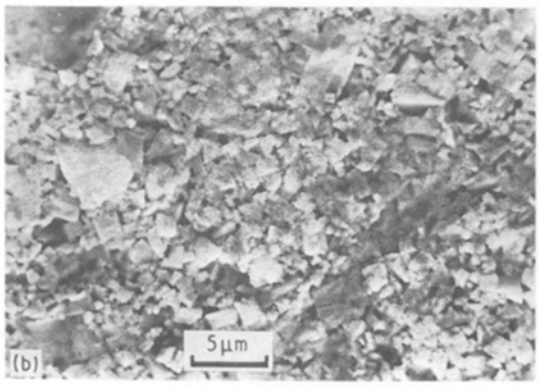

Figure 5 Surface structure of Spot I. (a) Optical micrograph of the laser Spot I showing the low-temperature area (LTA, bright region) and the high-temperature area (HTA, dark region). The very dark areas mark the regions observed by the APC. (b) Surface structure in the LTA (marked area in (a), scanning electron micrograph). (c) Surface structure in the HTA (marked area in (a), scanning electron micrograph.

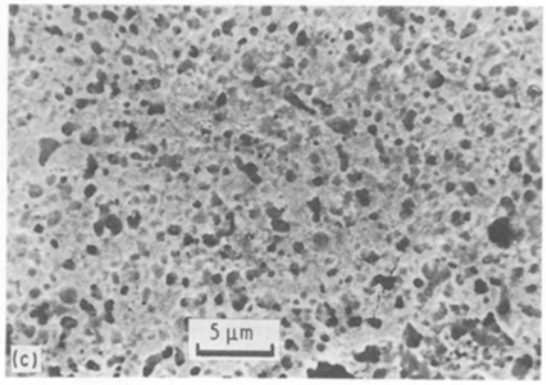

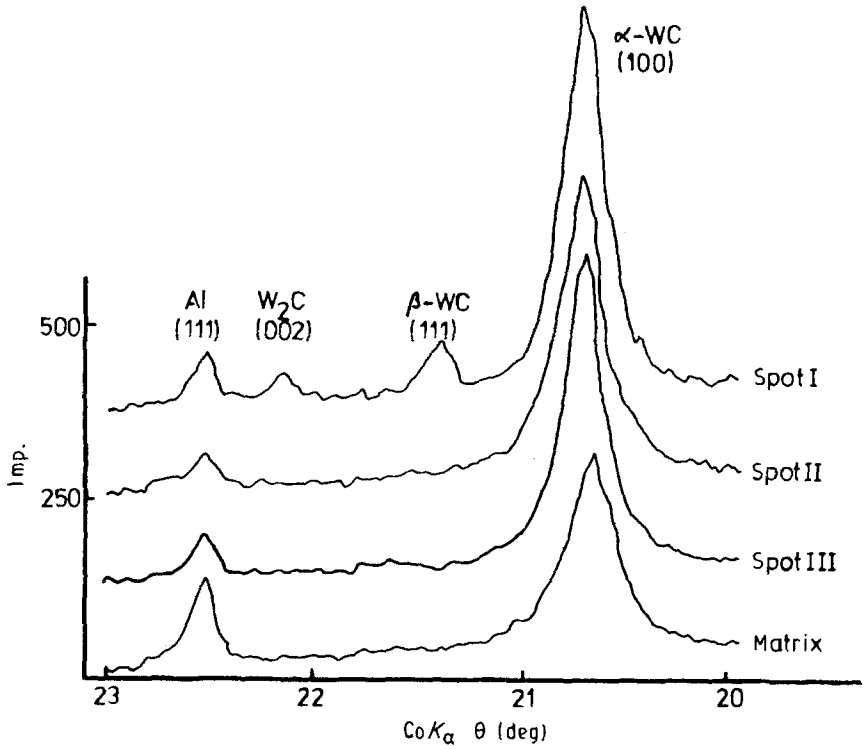

Figure 6 Qualitative phase analysis of the irradiated spots, simultaneously detected by PSD. The Al(1 1 1) reflection is based on a small quantity of aluminium used for marking the actual observed sample region, see Fig. 2.

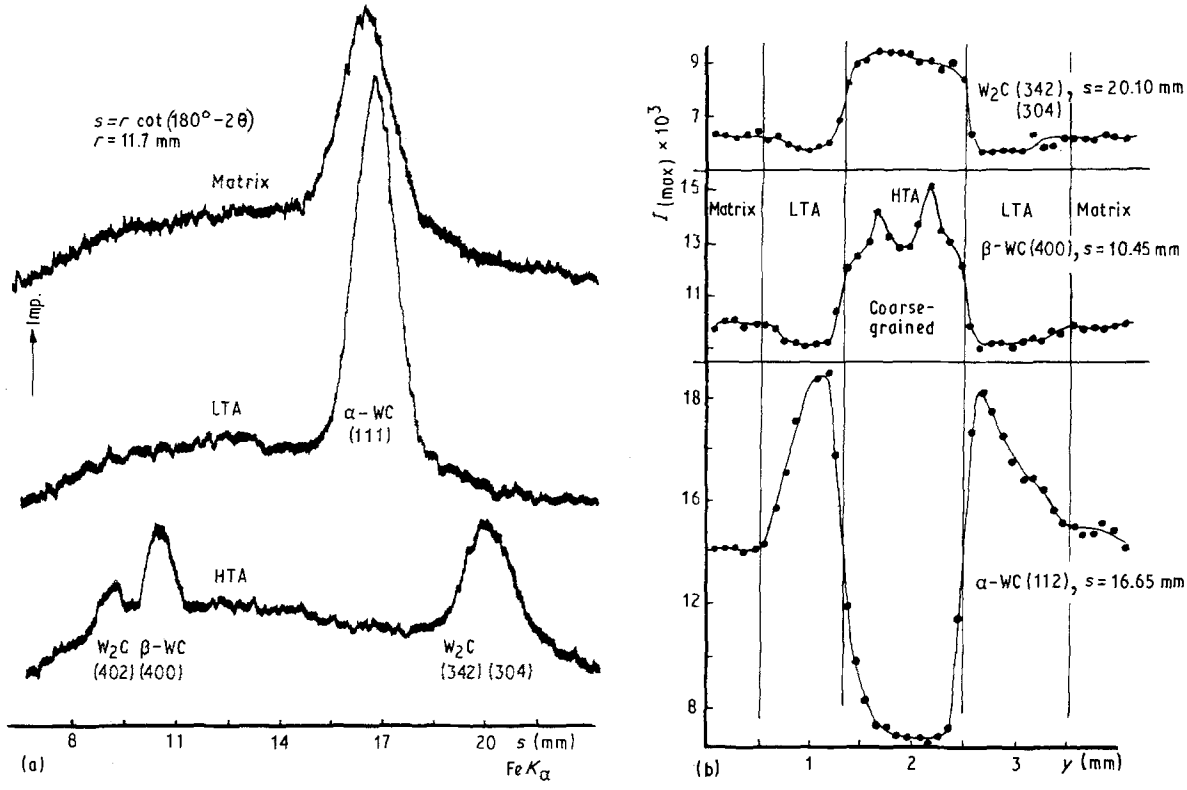

Figure 7 Qualitative phase analysis in the dark region of Spot I: (a) versus distance, s, sample–APC; (b) versus stepwise, Δy, movement of the sample for fixed s values per reflection (see (a)).

by Binden and Macherauch [9]. The main topic is that the intersection point of the $\sin^2\psi$ lines for variable surface stresses leads to s^*, which corresponds to the nondilated d-value, d^*. The small rectangle in Fig. 8a marks the weighted average for this point (with error limits). Inside the LTA region of Spot I, differences in stress between the axial and the tangential direction were observed. In this case the average value was used, following the theory.

In a more convenient way, s^*, is also the intersection point of the line of the b_0 values versus the different b_1 belonging to them (Fig. 8b),

TABLE I Apparent lattice parameters of α-WC and values of $d(1\,1\,2)$

		Matrix	Spot I[a] (LTA)	Spot II	Spot III	Powder (for comp.)
PSD (1 1 2), (2 0 1)	a (nm)	0.291 4	0.291 2	0.291 2	0.290 9	0.2906(3)
	c (nm)	0.283 5	0.283 5	0.283 4	0.283 5	0.283 7(2)
APC ($\psi = 0°$)	d (112) (nm)	0.101 65	0.101 54	0.101 54	0.101 49	0.101 53

[a] For PSD measurements a matrix overlap cannot be excluded.

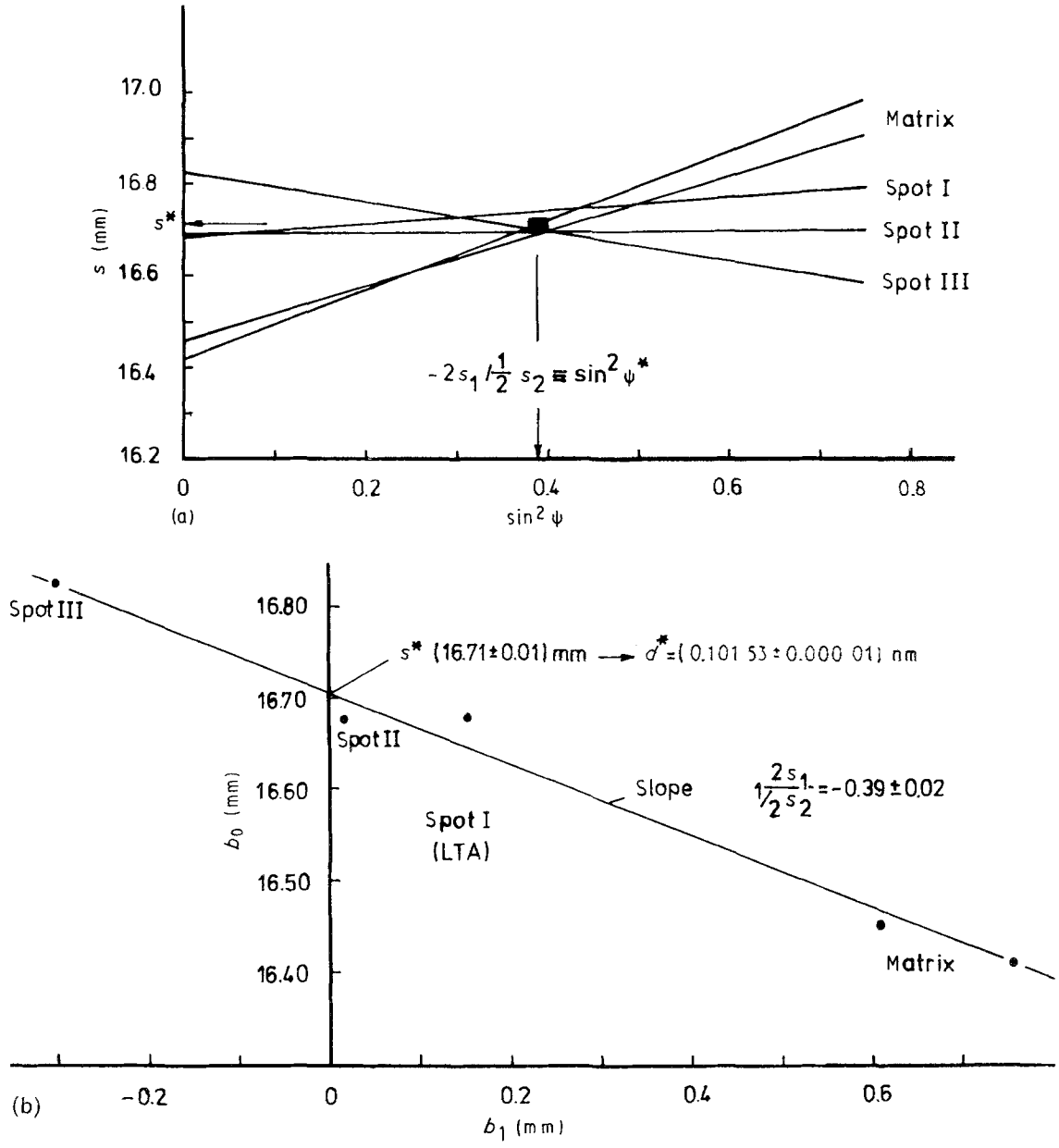

Figure 8 Results of stress measurements on α-WC by APC in the matrix (two measurements) and Spots I, II, III (reflection (1 1 2), FeK_α radiation). (a) Position s of the peak maximum versus $\sin^2\psi$ (linear regression lines). The dark region marks the error area of the intersection points; (b) following the method of the nondilated direction.

$b_0 = s^* + 2b_1 s_1/0.5 s_2$. The slope of this line is the same as the $\sin^2\psi^*$ in Fig. 8a

$$-\sin^2\psi^* = \partial b_0/\partial b_1 = 2s_1/0.5s_2 \simeq 2\nu/(1+\nu) \quad (1)$$

where ν is the Poisson parameter in the isotropic case. Consequently, ψ^* is the angle at which the unstressed lattice parameters can be measured. The determined s^* leads to $d^* = 0.101\,53$ nm, precisely the value for stoichiometric α-WC. From this the important fact follows, that the various lattice parameters in the spots are only based on different stress states, and the stoichiometry of the α-WC was not influenced by laser treatment. This points to the strong stoichiometry of the α-WC up to high temperatures as well.

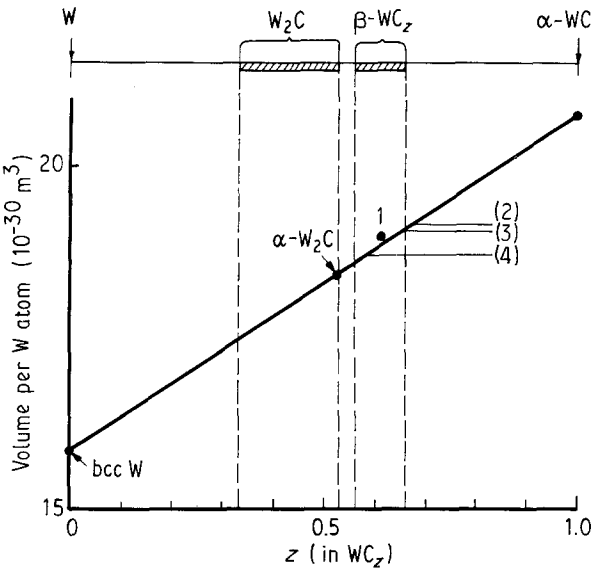

Figure 9 Relation between lattice volume per W atom and carbon content, z (corresponding to WC_z) of the W–C phases, phase limits after Rudy and Hoffmann [10]. β-WC_z: (1) [10], (2) [12], (3) present work, (4) [11].

The degree of decarburization of the phases inside the molten area of Spot I was also investigated. Stress measurements at the reflections W_2C (1 0 4) and β-WC_z (2 2 2) (CrK_α radiation) show no significant residual stress. Evidently, the tensile stresses primarily built up by high-temperature creep have relaxed by crack formation (Fig. 5a). For the W_2C phase the observed value $d(1\,0\,4) = (0.112\,522 \pm 0.000\,02)$ nm coincides with that for the stoichiometric composition. For the cubic β-WC_z (reflection (2 2 2)) a lattice parameter $a = (0.4239 \pm 0.0001)$ nm was measured. For determination of the stoichiometric coefficient, z, the plot represented in Fig. 9 was used. There the dependence of lattice volumes per W atom, V, for the W–C phases on z are given. Marked points are the standard volumes of b c c W ($a = 0.316\,48$ nm; $V = a^3/2 = 0.015\,85\,nm^3$, the stoichiometric hexagonal W_2C ($a = 0.299\,71$ nm; $c = 0.472\,81$ nm; $V = (3^{1/2}/4)\,a^2c = 0.018\,39\,nm^3$) and the hexagonal α-WC ($a = 0.290\,62$ nm, $c = 0.283\,78$ nm; $V = (3^{1/2}/2)\,a^2c = 0.020\,76\,nm^3$) as they are given by the JCPDS Data. The relation between this lattice volume and carbon fraction, z, is very well fitted by a straight line over the whole region between W ($z = 0$) and α-WC ($z = 1$). The value for β-$WC_{0.61}$ ($a = 0.422$ nm) determined by Rudy and Hoffmann [10] by careful measurements fits on to this line, too. In general, the direct correspondence with the original carbon content by the high-temperature phase is problematic because of carbon separation during the molten state which usually appears [10, 11].

The lattice volumes for β-WC_z with uncertain carbon contents produced by different methods are also plotted. On soft quenching in liquid tin, $a = 0.4215$ nm (corresponding to $V = 0.018\,72\,nm^3$) is obtained [11] and on hard quenching by electro-erosive processing $a = 0.4248$ nm ($V = 0.019\,16\,nm^3$) [12]. According to the straight gauge curve these values correspond nearly to the carbon-poor ($z = 0.59$) and carbon-rich ($z = 0.68$) side of the β-WC_z existence region. This result is consistent with the decreasing extent of decarburization of rapid thermal treatment. Our measured value of $a = 0.4239$ nm ($V = 0.019\,04$ nm^3) corresponds to $z = 0.66$ after laser treatment and approximates that of the comparable electro erosion. This means that both phases W_2C and β-WC_z, coexisting in the HTA, in our case are at the carbon-rich limit of their phase regions, whereas the carbon-rich W_2C and strongly decarburized β-WC_z should be in equilibrium. This contradiction may be a hint of the extreme non-equilibrium character of the laser-induced processes. Considering a comparable quantity of W_2C and β-WC_z, the resulting carbon fraction in the HTA is about $50[1/(1 + 2)] + 50[0.66/(0.66 + 1)] = 36$ at % C, compared with 50 at % C in the starting α-WC.

4. Conclusions

It has been shown that with suitable detectors, small regions, e.g. laser-treated areas, can be investigated in a comprehensive way. The advantages of a PSD were used down to 3 mm^2. Measurements with a micro-diffractometer and an APC ensured precise information in regions of 0.04 mm^2. After laser treatment of an α-WC–6%Co system, the high-temperature state was frozen. In the molten area only hexagonal W_2C and cubic β-WC_z were observed, consequently no decay of β-WC_z into α-WC and W_2C had occurred. The changes of the lattice parameters of the α-WC could be attributed to different residual stress fields without any change in its stoichiometry. This result was found by the generalized nondilated direction method. This means that the existence of α-WC shown in Fig. 1 should be replaced by a line. The degree of decarburization of the molten area was estimated from the lattice parameters and leads to a carbon content of 36 at % C with a high-temperature phase, β-$WC_{0.66}$.

References

1. B. SCHULTRICH, H.-J. SCHEIBE, H. MÜLLER, M. ERMRICH, G. KEßLER and E. DIEßNER, *Rev. Roum. Phys.* **34** (1989) 945.
2. B. SCHULTRICH and K. WETZIG, *J. Mater. Sci.* **22** (1987) 3361.
3. H. MÜLLER, K. WETZIG, B. SCHULTRICH, S. M. PIMENOV, N. I. CHAPLIEV, V. I. KONOV and A. M. PROCHOROV, *ibid.* **24** (1989) 3329.
4. *Idem., ibid.* **25** (1990) 4440.
5. B. O. JAENNSON, *Mater. Sc. Engng* **8** (1971) 41.
6. M. ERMRICH and K. RICHTER, *Wiss. Berichte ZFW Dresden, Acad. Sci. GDR, Heft* **30** (1988) 163.
7. *Idem., Mitt. VFK DDR, Heft* **2** (1989) 10.
8. D. STEPHAN and K. RICHTER, *Cryst. Res. Technol.* **16** (1981) K57.
9. F. BINDER and E.MACHERAUCH, *Arch. Eisenhüttenw.* **26** (1955) 541.
10. E. RUDY and J. R. HOFFMANN, *Planseeber. Pulvermet.* **15** (1967) 174.
11. R. V. SARA, *J. Amer. Ceram. Soc.* **48** (1965) 251.
12. E. KRAINER and K. ROBITSCH, *Planseeber. Pulvermet.* **15** (1967) 46.

Received 28 January
and accepted 7 June 1991